Electric Field Controlled Synthesis of Carbon Nanotubes

Alexandre Vaz Gamboa Sanches
alexandre.gamboa@tecnico.ulisboa.pt

Instituto Superior Técnico, Lisboa, Portugal

December 2019

Abstract

Since the discovery of CNTs in 1991, research in this material has risen exponentially. There are several alternatives when it comes to production methods, however, these are generally very costly and time consuming. Flame synthesis emerged as an alternative, seeing that cost-effectiveness is class leading, it is scalable, energy efficient and fast. A premixed Propane/Air flame with inert co-flow was employed, along with a moderate DC electric field to assess the effect on mass production and morphology of CNTs yielded with electric bias. Reynolds numbers of 250, 300 and 400 were analysed, seeing that these values provide an envelope flame shape favourable towards CNTs production. A supported plate of 303L stainless steel acted as the substrate. Mass measurements were performed, and it was concluded that applying voltage to the substrate results in increase of mass production. For all the conditions tested, applying 30V to the substrate proved to be the optimal situation regarding mass production improvements. On the other hand, negative voltages showed no signs of significant mass gains and revealed some inconsistency, showing different behaviours for distinct Reynolds. It was observed that the expected diameter decreases when voltage is applied to the substrate and that catalytic activity is enhanced. Temperature measurements and PIV analysis lead to the conclusion that the presence of the electric field does not affect the mixture flow. Moreover, the mechanism of mass growth rate revealed to be similar whether E is present or not and a monomolecular model was proposed for its description.

Keywords: Carbon Nanotubes, flame synthesis, electric field, particle image velocimetry, premixed flame.

1. Introduction

Nanoscience and nanotechnology have emerged in the last decade as a promising area, opening a wide spectrum of applications to the world of engineering. The estimations available expect that this sector will be valued at 125 billion USD by the year 2024 while still following an increasing tendency [5].

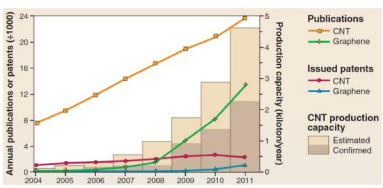

Figure 1: CNTs production, annual publications and patents issued between 2004 and 2011. Adapted from [6].

Carbon Nanotubes (CNTs) are amongst the most promising novel nanomaterials with excellent properties, earning in fact the designation of "material of the 21st century" [11]. Between 2004 and 2011 the annual publications issued worldwide tripled as visible in Figure 1, however, the knowledge and technical understanding for producing carbon nanotubes in large scale applications is still in development [6].

There are a few methods currently available for production of CNTs such as Chemical Vapour Deposition (CVD), Laser Ablation (LA), Electric Arc Discharge (AD) and Flame Synthesis. It is important to refer that the first three methods mentioned all have one drawback, an external source of energy has to be present making them costly processes. Flame synthesis appears amongst the methods mentioned as a novelty, nonetheless, production of CNTs through this technique has tremendous potential. The flame environment provides an ideal scenario while being cost and energy efficient, scalable and a continuous process [3].

Controlling and understanding the growth process of CNTs is important to definitely establish flame synthesis as an accredited method. The application of an electric field has emerged as a possibility to enhance the quantity and the properties of the yielded products, meaning the actuation and

details of this method require research.

2. Background

2.1. Carbon Nanotubes

Carbon hybridization is important for the morphology of carbon structures. When the C-C bond assumes a sp^2 configuration the resulting product is graphene, which corresponds to a single layer of carbon atoms arranged in a honeycomb lattice. Carbon nanotubes can be visualized as graphene sheets that rolled themselves into a tube shape, resembling an elongated C60 (buckminsterfullerene) [2].

CNTs are divided into Single Walled Carbon Nanotubes (SWCNTs) and Multi Walled Carbon Nanotubes (MWCNTs). The former consists of a single layer of graphene forming a hollow cylinder, usually with diameters in the order of 1nm. MWCNTs are the most common and effortlessly synthesized. These consist of several concentric layers of hollow cylinders with a separation between tubes similar to the inter-planar distance observed in graphite (0.34 nm). The diameters of these nanotubes range from 2 to 100 nm [10]. Both types are clearly represented in Figure 2.

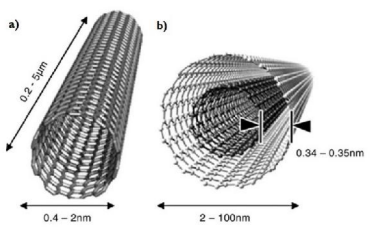

Figure 2: Single-Walled and Multi-Walled Carbon Nanotubes. Adapted from [10].

2.2. Flame Synthesis

CNTs can be synthesized using different types of flames. Premixed flames, normal diffusion flames, counter flow diffusion flames, co-flow diffusion flames and inverse diffusion flames have been exploited for nanotubes production. Premixed flames offer exclusive advantages that makes them the perfect candidate for studying the growth process of CNTs. A variety of fuels can be selected, the adjustability of the reaction gases stoichiometry allows for great flame control and the setup can be designed for a continuous scalable process. Height et al. in 2004 [9] investigated parameters such as CNTs growth zone, time scales and CNTs structures using a premixed flame of acetylene, oxygen and 15 mol% argon while using $Fe(CO)_5$ as a catalyst. The conclusion was that CNTs were synthesized with equivalence ratio (ϕ) between 1.5 and 1.9, with better results near the bottom of the equivalence ratio window. In 2017, Chong et al. [4] studied the formation of CNTs using a propane rich premixed flame. Results proved that the method is suitable for MWCNTs synthesis.

Nanotube synthesis with influence of a moderate electric field (E) was first introduced using flame synthesis by Merchan-Merchan et al. [12] who applied it when working with a counter diffusion methane flame. Potentials of only 300 mV were reported. Not only the presence of small aligned bundles of carbon nanotubes was detected in scanning electron microscopy (SEM) images, those were uniform in diameter. The growth rate and flame area suitable for production of CNTs were also improved. The authors also stated that the mechanism of actuation of E on the CNTs is due to polarization and the creation of a bound charge on the tip of the nanotube. The resultant electrostatic force can be decomposed in axial and tangential components as per Figure 3. The tangential force, $F_{TF} = qE\cos\theta$, has the role of orientating the CNTs while the axial force, $F_{AF} = qE\sin\theta$, stretches the tube and dampens the thermal vibrations CNTs are subjected to during synthesis.

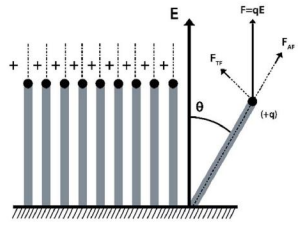

Figure 3: Electrostatic force acting on CNTs. Adapted from [8].

3. Implementation

The combustion system utilized throughout this experiment consisted of a Bunsen burner, mass flow meters and all the reactant gases required to establish the premixed flame, a DC power supply and an oscilloscope. To analyse the flame temperature a thermocouple was installed and a digital camera was used to capture images of the flame and deposited substrates. The schematic of the installation is provided in Figure 4.

3.1. Coordinates

A coordinate system is crucial to properly define not only the position of the substrate, but also the positions where the temperature is measured. Figure 5 depicts the coordinate system adopted. Points A to F are the points where temperatures were measured.

The origin of our referential is coincident with the centre of the outlet nozzle and the height of the substrate is defined as height above burner (HAB). For z=0 corresponds HAB=0.

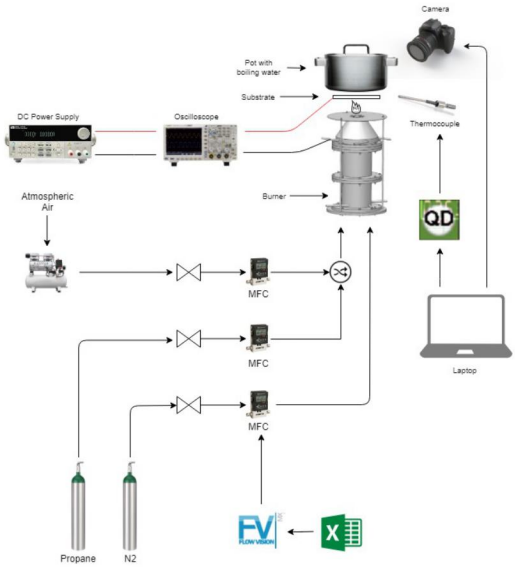

Figure 4: Combustion system schematic.

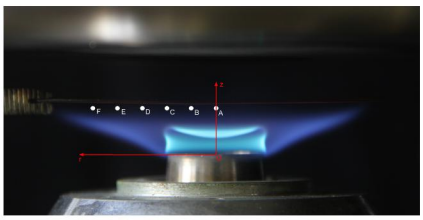

Figure 5: Flame coordinates (r, z) in millimetres. The coordinates for each point are: A(0,10), B(5,10), C(10,10), D(15,10), E(20,10), F(25,10)

3.2. Electric System

The voltage was supplied by a DC power supply branded Tektronix PWS2326. This equipment has voltage capabilities ranging from 0 to 32V. The power supply was connected to an oscilloscope (Tektronix 1001C-EDU) so that the voltage supplied could be constantly monitored. From the oscilloscope, the substrate and the burner were connected according to the experimental conditions specified. A positive voltage refers to the substrate being charged and the burner grounded while negative voltages refer to the opposite scenario. For verification, a multimeter was also available.

3.3. Particle Implementation Velocimetry

In order to understand the influence of the electrostatic force on the flow, the particle implementation velocimetry (PIV) is a very useful, precise and non-intrusive tool. The system takes measurements by aiming a double pulsed laser at seeding particles injected in the flow. The laser can be described as a planar sheet of green light, with a wave length of ≈530 nm, aimed at the flame. The particles are illuminated in two consecutive instants registered by a high-speed sCMOS camera. Therefore, two frames consisting of multiple images are obtained that allow the extrapolation of the mean velocity field. The time span between frames is defined and the distance travelled is calculated from the difference between frames, meaning that a velocity field can be attained. For the purpose of our analysis, alumina seeding particles with diameter of 3μm were selected. These were placed in a small reservoir while being constantly agitated, so that adequate dispersion was achieved.

The laser was a Dantec Dual Power 65-15 Yag, which has two cavities with 15 Hz of maximum laser pulse frequency each. The camera (HiSense Zyla sCMOS) was perpendicular to the laser sheet for proper recording of images. To avoid excessive light and ensure only green radiation hits our target, a 532nm Melles Griot filter was placed appropriately. To accomplish synchronization between the laser and camera, a BNC 575 Series Pulse Generator combined with Dantec Dynamic Studio was utilized. The working conditions for PIV measurements were Reynolds number of 300 and HAB=10mm. In Figure 6 is displayed the schematic of the PIV installation.

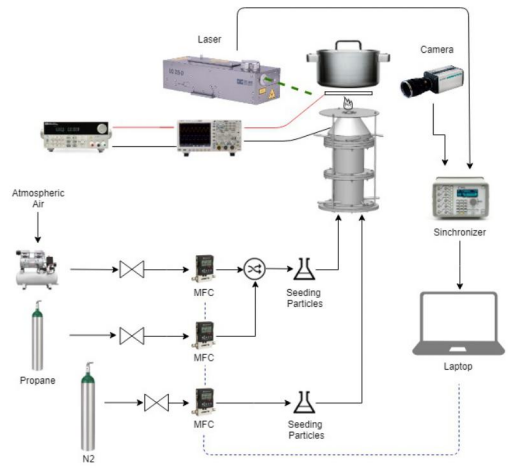

Figure 6: PIV experimental setup.

The 2D velocity fields are obtained by an average correlation method. This means that, for each interrogation area (IA), a correlation function is averaged at each location for every image. The IA defined for our experiment was sized 32 by 32 pixels. Another user input that must be defined is the time between pulses. An accurate selection is crucial to obtain trustworthy results. If the interval is set too low, the particles may not have enough time to move and very small vectors are extrapolated. If the time frame is set too high the particles may travel distances long enough that by the time the second frame is captured the particle is outside

the interrogation area. It is important to note that in each IA, for the first frame, there will be particles close to the edge that unavoidably will dislocate to another IA. This aspect can be bypassed by setting an overlapping factor. In this experiment, an interval of 200 μs and an overlapping factor of 50% x 50% were selected.

3.4. Premixed Flame

To establish the flame the following procedure was followed. Firstly, all the mass flow controllers are connected to the laptop, the software Flowvision is turned on, and the connection between laptop and flow meters is configured. Subsequently, all the security valves for C_3H_8 and air are opened. Then, the N_2 bottle is opened, with the pressure set to 2 bar. With all the valves opened, the values for all the mass flows are input to Flowvision, a few seconds are allowed so that the gas flow reaches the outlet and then the flame is ignited. From here, both the power supply and oscilloscope are turned on, followed by the introduction of the voltage selected for the trial. When the water in the pot is boiling, the substrate is placed in the three-way translator. The voltage between the substrate and the burner is checked with the multimeter, and if everything is in conformity to trial conditions the substrate is placed in the desired HAB and radial position over the flame. After the specified experimental time the substrate is removed from the flame and set aside for cooling. If there are no more trials to be conducted the flame is extinguished and all valves and handles are closed. The electrical equipments and flow meters are turned off for completion of the process.

3.5. Substrate Preparation

Throughout the entirety of this work two types of substrates were used, stainless steel and coated stainless steel. The former was annealed stainless steel (SS) that was sanded with 120 grit sandpaper (Dexter brand) and cleaned with acetone before every experiment. All these plates were used multiple times. The latter consisted of stainless steel coated with zinc and cobalt derived materials that were electrodeposited on the stainless steel substrates.

3.6. Zinc and Cobalt Electrodeposition

Zinc and cobalt derived materials were electrodeposited on two stainless steel plates prepared as described in Subsection 3.5. All the experiments were carried out at room temperature, by connecting both the substrate and the graphitic electrode to a Kikusui Electronics PAB32-3 power supply. The parameters used were a current of 1 ampere and a working time of 2 minutes. The Power Supply also displayed a voltage of 3.4V.

The solutions of zinc and cobalt were prepared using analytical grade chemicals and distilled water. For both electrolytic solutions 1L of solution was prepared. For zinc, 0.5M of $ZnCl_2$ (zinc chloride) and 2M of NH_4Cl (ammonium chloride) were present in the solution. For the cobalt solution, this was prepared with $CoCl_2$ (cobalt chloride), NH_4Cl and NaCl (sodium chloride).

3.7. Working Conditions

Initial tests were performed to evaluate how formation of CNTs occurred. HAB was varied from 4 mm to 16 mm and ϕ of 1.6 and 1.8 were tested. Inert dilution of nitrogen was set at 0.1 LPM. From visual and mass measurements HAB was set at 10mm and ϕ of 1.6 was adopted. The voltages applied ranged between 0 and 30 volts.

As in all flows, there is a convective force associated with the mass and movement of particles. This force may compete with the force exerted by the electric field, consequently the variation of Reynolds and Voltage applied had to be studied so that conclusions about the effects of E on mass produced and morphology of resultant CNTs could be withdrawn. The first step was to assess the conditions where it was possible to establish an envelope flame that was previously known to be favourable towards CNTs synthesis. Starting at Re=150 and up to Re=430 it was possible to have an envelope flame. However, for Reynolds lower than 250, the flashback risk was high. For Reynolds higher than 400, the flame was not stable. Three values of Reynolds, 250,300 and 400, were selected to be tested at voltages of 0, ±1, ±10, ±20 and ±30 volts and a fixed sampling time of 15 minutes.

For negative voltages, for both 250 and 400 Reynolds values, there was no clear tendency between mass produced and voltage. Also, only for positive voltages of 20V and 30V there were significant gains of mass production. Re=300 revealed some insensitivity to polarity change, with mass increments registered for both negative and positive voltages.

Due to the facts mentioned above, and also to compare with the results of Duarte [7], Re=300 was the condition chosen to perform a time analysis in order to examine how the implementation of E affected the mass growth rate of CNTs. Voltages of 20V and 30V were applied. Sampling times of 5, 10, 15, 20, 30, 40, 50, 60, 70 and 90 minutes were analysed.

Regarding the catalyst deposited substrates, these were tested for 10 minutes under a 30V bias. For economical and time reasons, only one test was performed with coated substrates. Reusing bare steel plates allows repeatable and affordable production. For PIV and temperature measurements, these were performed for Re=300 and for all the

voltages tested.

3.8. Characterization of CNTs

X-ray diffraction (XRD) was used to obtain structural informations that allow the description of the substrate and yield products. The crystalline structure of the stainless steel plates and deposited materials was assessed through SEM (Hitachi S2400 or FEG-SEM, JEOLJSM7001F).

4. Results

4.1. Substrate Description

From the substrate XRD it was concluded that mostly Austenite (γ-Fe) composed the material. An EDS was also performed and reported that the steel had a weight composition of 17.5% Chromium, 7.8% Nickel and 1.8% Manganese. From these values one can conclude that the substrate is an austenitic 303L stainless steel.

4.2. Synthesis Without Electric Field

Re=300 was the initial working condition upon which this work started to analyse synthesis without application of E. Mass measurements and SEM characterization of the yielded CNTs was made. An average of 5.2 mg of CNTs was achieved for sampling time of 15 minutes. Using iTEM software, an expected value for the diameter of the nanotubes was calculated via the implementation of a normal distribution based on 60 values of measured diameters. Both the SEM image and diameter distribution of CNTs are visible in Figure 7. An expected diameter of 59.95 nm was attained.

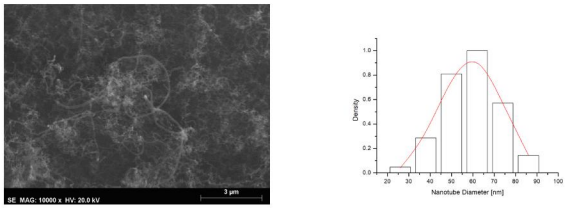

(a) SEM (b) Diameter Distribution

Figure 7: SEM image at 10K magnification of CNTs produced without electric field and respective normal distribution of the diameters.

The masses and deposition areas for the different Reynolds analysed in this work were also studied. The former were extrapolated from binarized photographs of the substrate after deposition using the software ImageJ. In Table 1 are displayed the values of mass production and deposition areas for Reynolds numbers of 250, 300 and 400 with no voltage applied for a sampling time of 15 minutes.

XRD analysis was performed on synthesized CNTs. Peaks related to graphitic (002) and (100) lattices were registered. The (002) peak is associated with the inter-planar graphitic distance of 0.34 nm, which is the characteristic separation between the concentric tubes in MWCNTs, confirming that in fact MWCNTs were synthesized.

Table 1: Mass and deposition area measurements without electric field for Re=250, 300 and 400.

ϕ	HAB [mm]	t [min]	Re	Mass [g]	Area [cm^2]
1.6	10	15	250	3.8	9.52
1.6	10	15	300	5.2	19.46
1.6	10	15	400	5.9	19.74

4.3. Electric Field Simulation

A simulation was performed to evaluate the electric field established. A 3D CAD model of the top section of the burner was designed, and a stainless steel plate was introduced at HAB=10mm to create a realistic assembly of our setup. The electric field was simulated for ±1V, ±10V, ±20V and ±30V.

From the results we can affirm that the electric field near the substrate is uniform and perpendicular to the plate, with the field lines leaving the substrate towards the burner. This was the case for all the positive voltages with intensity according to the voltage. In Table 2 the different E magnitudes are available.

Table 2: Average magnitude of E for the different voltages applied based on simulation results.

$\triangle V$ [V]	E [V/m]
1	74.4
10	771.4
20	1629.6
30	2414.3

For negative voltage E maintains uniformity near the substrate. The direction however is inverted because of the opposite polarity.

4.4. Influence of E on Mass Yield

Re number of 250 provides an outlet velocity for the mixture of 0.19 m/s, which translates into the lowest convective forces between the Re values selected. The evolution of mass production with the variation of voltage is depicted in Figure 8.

The average value for mass production with no voltage was 3.8 mg, which is in line with the value obtained for both 1 and 10 volts. When 20V were applied mass production increased from 3.8 mg to 5.2 mg. Further augment in the potential difference to 30V provided 7 mg of CNTs. This translates to a 37% and 84% increase in mass production, respectively. In regards to negative voltages, despite a very slight increase in mass being documented, there was no clear relationship between the varia-

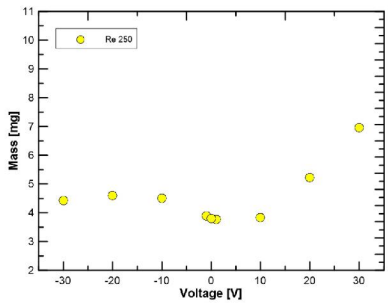

Figure 8: Mass measurements for production of carbon nanotubes with 0, ±1, ±10, ±20 and ±30V, for a *Re* number of 250.

tion of voltage and mass weighed after 15 minutes. The average mass measurements for -1, -10, -20 and -30 were 3.8, 4.5, 4.6 and 4.4 mg, respectively.

For *Re*=300 the outlet velocity of the mixture is 0.23 m/s, thus having slightly higher convective forces than the previous case. Results are available in Figure 9.

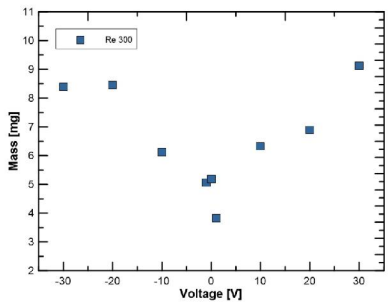

Figure 9: Mass measurements for production of carbon nanotubes with 0, ±1, ±10, ±20 and ±30V, for a *Re* number of 300.

Mass production without voltage for this condition was 5.2 mg. Starting with the positive side, applying 1V resulted in decrease of mass production from 5.2 mg to 3.8 mg, although this value is most likely an error associated with the burner. At 10V, the yield was 6.3 mg (22% increase), at 20V 6.9 mg (33% increase) and at 30V 9.1 mg (75% increase) were obtained. For negative voltages, the tendency of the mass produced was to raise when the magnitude of the electric field was raised (absolute value). At -1V there were no mass gains, for -10V an increase of 0.9 mg (17%) was obtained, for -20V, 8.5 mg of CNTs were measured and stagnation appeared to occur, since the mass for -30V remained almost constant at 8.4 mg, representing a 63.4% raise. With these results, it is concluded that *Re*=300 is relatively insensitive to polarity as well as requiring lower positive voltages to register a significant mass increase compared to *Re*=250.

The last value of Reynolds subjected to this same experiment was 400. With an outlet velocity for the mixture of 0.3 m/s, the respective flow has the highest convective component from all the values presented above. The results are plotted in Figure 10.

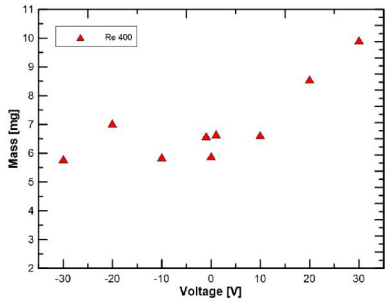

Figure 10: Mass measurements for production of carbon nanotubes with 0, ±1, ±10, ±20 and ±30V, for a *Re* number of 400.

At 0V *Re*=400 yields 5.9 mg, 1V produced 6.7 mg of carbon nanotubes and for 10V the increase in voltage did not reveal any additional gains in mass, with 6.6 mg. When 20V and 30V were applied, production of 8.6 and 9.9 mg was measured for each situation. On the negative side of the voltage axis, the situation was resemblant of the *Re*=250 case. There is no defined relationship between voltage variation and mass production. The mass results for -1, -10, -20 and -30V are 6.6, 5.9, 7 and 5.8 mg. The maximum increase was achieved for -20V, a 19% gain.

The results above are intriguing, seeing that for negative voltages there is a difference between the outcomes obtained with different *Re* values. For *Re*=300, negative bias has the capability of increasing mass production in significant amounts, although not as much as the positive equivalents. For *Re*=250 and *Re*=400 that was not the case. In search of an explanation for the statements above, the deposited areas for the different conditions were investigated, particularly to understand the evolution when negative voltages are applied. From the deposition area analysis it was concluded that the mechanisms of deposition are different for *Re*=250/400 and *Re*=300. When no electric field is applied, for the first cases, the deposition area consists of a circle in the centre and an outer crown with thickness of ≈3 to 5 mm. For Reynolds number of 300 the deposition area covers a wide span of radial coordinates with more uniform coverage. The difference is visible in Figure 11.

When positive voltages of 20V or higher were applied, the deposition area for *Re* 250 and 400 suffered a shape change to a uniform dense coverage similar to that of *Re*=300. For negative voltages the shape change was not present. This indicated that only positive voltages were capable of significant mass increases because of the ability to in-

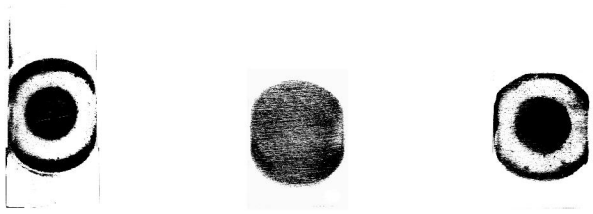

(a) 250 (b) 300 (c) 400

Figure 11: Binarized photographs of deposited substrates for the different *Re* and 0V. The black areas correspond to deposited CNTs.

duce the deposition area alteration. This results are depicted in Figure 12. For *Re* 300 there was no shape change and the higher the voltage the denser the deposition became, indicative that this flow has the optimum conditions in terms of surface coverage. The different deposition behaviours somewhat isolates this case from the remaining, thus the existence of a different pathway for the mass deposition.

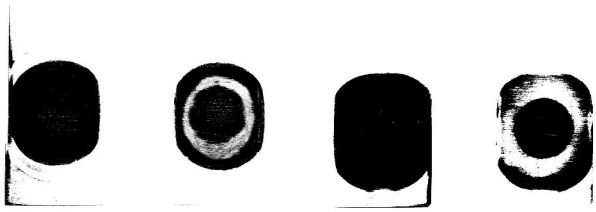

(a) 30V (b) -30V (c) 30V (d) -30V

Figure 12: Binarized photographs of deposited substrates for *Re* 250 (a,b) and 400 (c,d) at ±30V.

According to the work of [13], the breakdown of hydrocarbon molecules in the reaction zone culminates in the appearance of free radicals such as CH^-, $C{\equiv}C^-$ and C^-. These molecules suffer attraction from the positive plate and are the reason for the enhancement of mass production.

4.5. Morphology

For *Re*=300 with voltages of 5, 20 and 30V, SEM and diameter measurements were performed. The SEM images were taken in the centre of the samples and for 30V are available in Figure 13 with the respective diameter distribution. The expected diameter and diameter range for all the situations is found in Table 3.

Table 3: Expected diameters and diameter intervals for $\triangle V$=5, 20 and 30.

$\triangle V$ [V]	Expected Diameter [nm]	Diameter Range [nm]
5	56.21	29.23 - 76.97
20	52.62	32.64 - 75.57
30	39.89	26.14 - 66.66

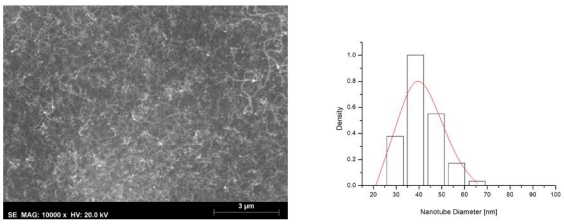

(a) SEM (b) Diameter Distribution

Figure 13: SEM image and diameter distribution for 30V.

It is concluded that the expected diameter of the nanotubes decreases with higher voltage values and no signs of alignment are visible. The diameter of the nanotubes is defined by the diameter of the catalytic particles. For bare substrate synthesis the particles are related to the surface roughness of the material and a process denominated metal dusting. According to [14] the last process involves electron transfer, therefore it is suggested that E may interfere with the formation of the catalytic nanoparticles, ultimately altering their diameters. Another parameter that influences the catalytic activity is temperature, so measurements are relevant.

4.6. Temperature and PIV

Being a critical parameter on nanotube synthesis, temperature measurements were taken at 5 different locations spreading the deposition area mentioned in Figure 5. The temperatures were measured without electric field and with both 20 and 30V bias. The results can be assessed in Figure 14.

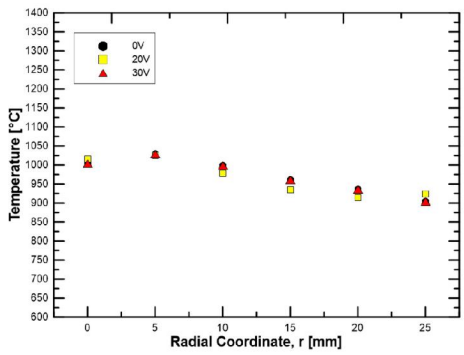

Figure 14: Temperatures measured at the five different locations with 0V, 20V and 30V applied to the substrate.

In general, the synthesis temperature is between 900°C and 1050°C. The results indicate that a moderate electric field has no effect on temperature. For 0, 20 and 30 volts, temperature values are extremely coincident, this indicates that gas phase in the reaction environment was not altered.

The flow characteristics are rarely debated in the scientific community when the mass production of

carbon nanotubes is of concern. However, velocities affect the residence time of carbonaceous materials near the substrate and affect the deposition process. To assess whether E has influence on the flow culminating in higher mass yield and larger deposition areas, PIV measurements were performed and 2D velocity maps for 0V and 30V are available in Figure 15. Only half the flow is presented due to radial symmetry.

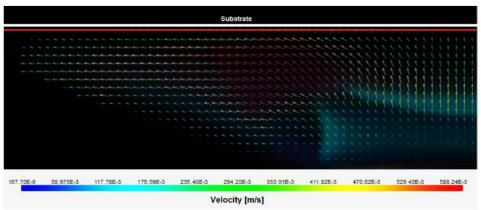

(a) 0V

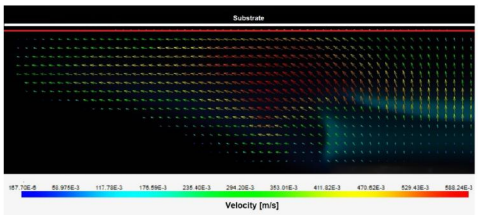

(b) 30V

Figure 15: 2D velocity map for the flow characterized by Reynolds number of 300 with 0 and 30V.

The velocity vector maps obtained are fairly similar in all the conditions which is indicative that the electric field magnitude is not sufficient to cause severe ionic winds. The velocities near the substrate, where potential alterations would have repercussions, were measured for every case and, despite minimal alterations, the values obtained are coincident. In the centre, r=0 mm, the velocities approach 0 m/s. From there, an increase up to 0.31 m/s, 0.33 m/s and 0.31 m/s for 0V, 30V and -30V, respectively, is observed. Those maximum values are obtained at r=10.5 mm. The velocity then decreases until r=27.5 mm where the velocities are approaching 0 m/s. It is concluded that E does not alter the flow, excluding this parameter of being the cause of mass gains and morphology changes.

4.7. Vertical Alignment

By simple observation of the SEM images obtained throughout our experiments, the CNTs produced do not show signs of alignment. Firstly, only top view images were possible to obtain with our substrate and SEM equipments. Ideally cross-section views would reveal in more detail the different orientations along the electrostatic force acting plane. In this study, a stainless steel substrate without any external catalyst is inserted in the flame, and both the tip and base growth mechanisms are observed. It is therefore likely that this setup does not grant the formation of vertically aligned CNTs, seeing that tip growth is required.

4.8. Time Analysis

CNTs growth is dependant on the catalyst particles and their ability to adsorb and diffuse carbon. As time passes, the solubility limits of the catalytic particles are reached, they become fully covered with carbon and diffusion no longer occurs. At this point the catalytic activity ceases. To assess the effect E exerts on the mass rate of carbon nanotubes and catalyst deactivation times the tests mentioned in Section 3.7 were performed. The results are plotted in Figure 4.8, where the data measured at 0V by [7] was also inserted for comparison. Values are an average of three experiments.

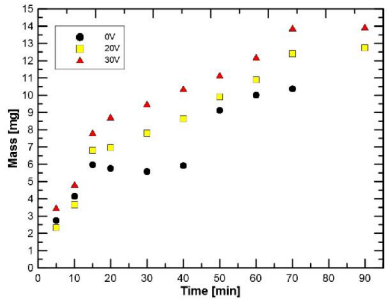

Figure 16: Mass measurements vs sampling time for 0, 20 and 30V.

In the 0V plot, two branches with positive growth rates, 0 to 15 minutes and 40 to 70 minutes are visible. From 0 to 15 minutes mass increased up to 5.98 mg where it stagnated. Only when the sampling time was 50 minutes mass gain was registered again, to a value of 9.1 mg. Subsequent increase in sampling time yielded higher mass production until 70 minutes when the growth ceased with a maximum mass of 10.1 mg. When 20V were applied, for 15 minutes, the mass produced was 7 mg and until there the growth rate was high. Stagnation was avoided and the mass increased continuously with a diminished rate that remained fairly constant until stagnation was verified at 70 minutes. The maximum yield registered was 13.1 mg, representing a 29.7% increase compared with the previous case. The behaviour when the bias was increased to 30V was very similar to that observed for 20V. For 30V important values to register are 7.8 mg at 15 minutes and a maximum production of 14.2 mg, representing an 40.6% gain relative to no voltage.

The mass increment came as no surprise. However, in the interval between 15 and 40 minutes E is able to maintain mass production gains with longer sampling times, contrarily to the 0V case. According to [7], from 0 to 15 minutes, only a small per-

centage of catalysts are active. Then, 40 minutes is the necessary period of time to activate the remaining catalyst particles. Based on a deposition area, diameter and temperature analysis, it was also concluded that with increasing sampling times the expected diameters of the nanotubes decrease. This means that large carbon nanotubes are the first to be formed and are subsequently covered with smaller ones, which transduces to bigger catalytic particles being readily active while smaller ones require larger periods of time to become active. From Table 3 it is seen the expected diameter of the samples decreases with increase in voltage. We can conclude with the combination of the diameter change, the mass increments and higher catalytic activity during the 15 to 40 minute interval, that voltages of 20V and 30V allow early activation of catalytic sites, meaning that even for lower sampling times the small nanotubes are already covering the bigger ones, hence why narrow expected diameters are extrapolated. If it is assumed that bigger catalytic particles have higher activity due to an increase of attraction forces between catalyst and carbon with particle size, the attraction induced by the electric field towards the substrate explains the early activation of smaller catalytic sites, as those need to exert less force to attract carbon.

To better compare the results all the curves were normalized. This means that two new variables are created to which the designation of t* and m* was attributed. For each experiment, the former corresponds to the sampling time divided by the stagnation time, while the latter is the mass obtained divided by the maximum mass for that condition. Because of the different branches in the curve with 0V, these were also divided into separate normalized curves. One with a saturation time of 15 minutes involving sampling times up to 40 minutes, and the second with a saturation time of 70 minutes involving sampling times between 40 and 70 minutes. The resulting plot is visible in Figure 17. For a complete analysis the results of all the trials performed are inserted in this graph, even though complete data for 0V was unavailable.

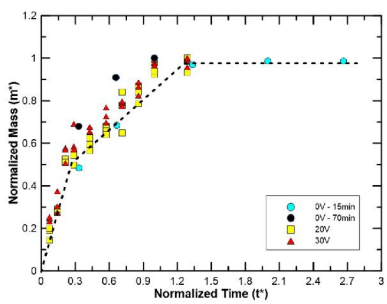

Figure 17: Normalized mass measurements vs sampling time for 0, 20 and 30V.

From the normalized plot it is withdrawn that the mechanism of growth rate for the different conditions lies in the same regime. The application of electric bias allows the maximum mass to be increased while the pathways up to those values remains consistent. Furthermore, the plot suggests three different behaviours highlighted by the three tendencies presented. For values of m*<0.55, the growth rate is high, i.e mass increase with sampling time is significant for the first 30% of t*. Beyond that point the growth rate diminishes until stagnation occurs where the growth rate becomes zero as CNTs production has ceased.

According to Bedewi et al. [1] the Gompertz model is the most suited to describe the growth dynamics of a population of carbon nanotubes. With this model it was not possible to obtain a good fit with our data seeing that all the possible curves did not pass through the origin of the plot, meaning that for t*=0 there was already mass produced, which is physically impossible. In the same report it is also mentioned that the monomolecular model may be employed. In an attempt to describe the dynamic growth obtained the monomolecular model was tested. An equation was found, however, it stands as a suggestion and not a definite model, since the normalized plot suggests three different growth rates with different characteristic equations. Nonetheless, with the monomolecular model the equation that best suits our data is characterized by α=0.9812, k=2.774 and τ=0, as per Equation 1. This model provides a confidence interval of 0.991. The resulting equation was plotted and the result is visible in Figure 4.8.

$$m^*(t) = 0.9812(1 - e^{-2.774t^*}) \tag{1}$$

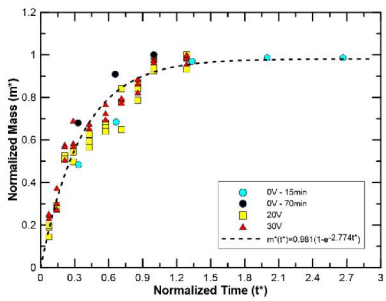

Figure 18: Fitment of the monomolecular analytical model to the results obtained in the experiments.

The plot suggests that the model provides good results, being coherent with the evolution obtained for the different conditions tested.

4.9. Deposited Substrates

Regarding the deposited tests, zinc revealed itself as unable to synthesize CNTs. For cobalt the re-

sults show an enormous potential for mass production. For 10 minutes 20 mg of CNTs were produced, which is more than the yield registered at 70 minutes for bare steel. Economical viability should be studied. Despite structural differences observed in SEM images, alignment of the CNTs was not apparent.

5. Conclusions

The major achievements accomplished upon conclusion of this study are enumerated below:

- Successful improvement of CNTs mass production via the implementation of a moderate electric field within the flame environment.
- Mass increments of up to 84% were registered when charging the supported substrate with 30V for a sampling time of 15 minutes, when comparing to synthesis without electric field.
- Proof that positive moderate voltages yield better results when compared to negative bias.
- Based on the results obtained, it was concluded that the presence of the electric field allows earlier activation of catalytic sites by attracting carbonaceous free radicals towards the substrate, hence the increase in mass produced.
- It was demonstrated that the electric field exerts no effects on the gas phase and temperature distribution in the flame environment, while also not influencing the mixture flow.
- An analytical monomolecular model was suggested to describe the dynamics of CNTs growth rates.

Acknowledgements

For all the support, the author would like to thank Prof. Edgar Fernandes, Dr. Luísa Marques, family and friends.

References

[1] M. Bedewy, E. R. Meshot, M. J. Reinker, and A. J. Hart. *ACS Nano*, 5(11):8974–8989, 2011.

[2] G. Bhat. In *Structure and Properties of High-Performance Fibers*, chapter 4, pages 79 – 109. Woodhead Publishing, 2017.

[3] J. Chen and X. Gao. *American Journal of Materials Synthesis and Processing*, 2(6):71–89, 2017.

[4] C. T. Chong, W. Hon Tan, S. Lee, W. Chong, S. S. Lam, and A. Valera-Medina. *Materials Chemistry and Physics*, 197:246–255, 2017.

[5] E. Comission. Nanotechnology – the invisible giant tackling europes future challenges. techreport, 2013.

[6] M. De Volder, S. Tawfick, R. Baughman, and A. J. Hart. *Science*, 339:535–539, 2013.

[7] A. F. K. Duarte. Master's thesis, Instituto Superior Tecnico, 2019.

[8] N. Hamzah, M. Fairus Mohd Yasin, M. Yusop, A. Saat, and N. A. Mohd Subha. *Journal of Materials Chemistry A*, 5(48):25144–25170, 2017.

[9] M. Height, J. Howard, and J. Tester. *Proceedings of the Combustion Institute*, 30:2537–2543, 2004.

[10] P. Kim, A. Majumdar, P. L. McEuen, and L. Shi. *Phys Rev Lett*, 87(21):215502, 2001.

[11] W. Merchan-Merchan, A. V. Saveliev, L. Kennedy, and W. C. Jimenez. *Progress in Energy and Combustion Science*, 36(6):696 – 727, 2010.

[12] W. Merchan-Merchan, A. V. Saveliev, and L. A. Kennedy. *Carbon*, 42(3):599 – 608, 2004.

[13] E. Plaza, H. Briceño, J. Arevalo-Fester, R. Atencio, and L. Corredor. *Journal of Nanoparticle Research*, 17(6):1–11, 2015.

[14] P. Szakalos. *Mechanisms of Metal Dusting*. KTH, 2004.